

Cubic Stress Tensor Sensor for Robot Skins

Shohei Kiyota¹ and Hiroyuki Shinoda¹

Department of Information Physics and Computing, The University of Tokyo, Tokyo, Japan

¹(Tel : +81-3-5841-6927; E-mail: {kiyot, shino}@alab.t.u-tokyo.ac.jp)

Abstract: The purpose of this research is to produce a sensor chip that measures a stress tensor in an arbitrary point in an elastic body such as an artificial skin for a robot. The sensor consists of a cube-shaped rigid body and sub-sensors that measure normal stress on each corner of the cube. We explain the theory to decompose shear stress and non-uniform normal stress. Also, we fabricate a prototype sensor. The theory is examined by the prototype. The experimental results show that the sensor can measure the normal stress and the shear stress at once. Also, the results suggest that the sensor can measure the gradient of contact surface.

Keywords: Tactile sensor, Elastic body, Stress tensor, Symmetric.

1. INTRODUCTION

In late years, to know a contact state with the object, many researches are conducted for measuring force vector distribution in fields of human interface and artificial skin for robots [1]. Many of force distribution sensors are commercialized as ones that measure only normal force distribution on the contact surface [2,3].

A Stress Tensor Sensor (STS) proposed in this paper is a small cubic sensing chip embedded in an elastic body for measuring all components of stress tensor around it. The usefulness of the tensor sensor is summarized as

- 1) Completeness of the information: Even if the STS orientation is arbitrary, any component of the stress tensor is calculated from the data of the STS. In order to measure a certain component of stress precisely, we need to consider the interference from other stress components. Usual sensors called a normal stress sensor also responds to other stress components if it is set in an elastic body. Measuring all components is a reasonable and probably the simplest way to decompose the stress component interference.
- 2) Directness of sensing: STSs are supposed to be placed near the surface, floating in an elastic body. In usual practical tactile sensing, the sensors are placed at the bottom of a thick elastic body. But the existence of the elastic body between the tactile sensor surface and the sensors lowers the spatial and temporal resolution of sensing the surface force distribution. In our STS sensing, the force on the surface is directly measured by the sensor chips floating near the surface.

The idea of the STS is already seen in some previous researches [5]. But it has not been considered as a practical method since it is difficult to wire the STS in an elastic body. However, the recent advancements of wireless networking technologies including two-dimensional signal transmission [6] makes it realistic to realize a wireless STS. This is the main motivation of the research.

The other problem of the previous STS is the

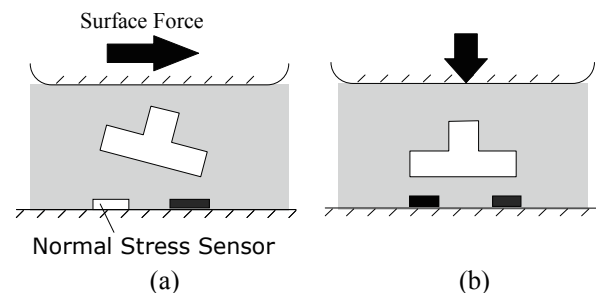


Fig.1 An example of the previously reported stress sensors. The sensor measures (a) the shear stress as the difference between the outputs of the sub-sensor and (b) the normal stress as the summation of the outputs of the sub-sensors. When the contact surface inclines, the sensor misinterprets the normal stress difference as the shear stress.

incompleteness of sensing. The previous sensor couldn't distinguish between the shear stress and the non-uniform normal stress. Fig. 1 illustrates a typical principle to measure the force direction seen in previous researches. Multiple normal stress sub-sensors and rigid body structure are embedded in an elastic body. This rigid body converts the tangential force on the surface into the normal force difference inside, and a force vector is calculated from the sum and a difference of the outputs of sub-sensor set at the bottom of the elastic body [4]. The normal force F_z and tangential force F_x on the surface are calculated as follows by the outputs of each sub-sensor V_1 and V_2 as

$$F_z = k_1(V_1 + V_2) \quad (1)$$

$$F_x = k_2(V_1 - V_2) \quad (2)$$

The constants k_1 and k_2 depend on the Young's modulus, poisson's ratio and the shape of the rigid body. This method is useful for the reason that it can get a force vector by adding a simple structure to conventional normal force distribution sensor. But the problem is that the sensor misinterprets the normal stress difference as the shear stress when the contact surface inclines.

In this paper, we present a sensing principle of STS free from the second problem. We fabricate a prototype and examine the principle.

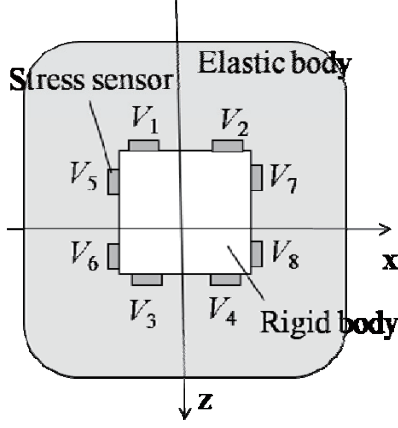


Fig.2 The schematic drawing of the sensor model. The white square indicates a rigid body.

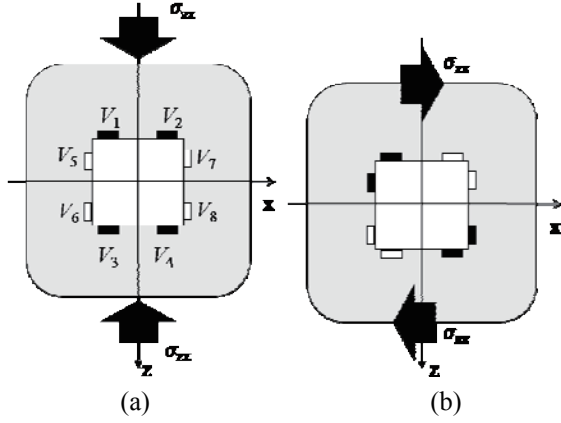


Fig.3 Normal stress distribution on the rigid body. (a) Even normal stress σ_{zz0} is applied. From geometrical symmetry, V_1, V_2, V_3 and V_4 are equally compressed, and also V_5, V_6, V_7 and V_8 are equally expanded. (b) The shear stress σ_{xz0} is applied.

2. PRINCIPLE AND SCALING LAW

For simplification of the following discussion, we first assume a 2D problem and focus on a cross section including the x - and z -axis as shown in Fig. 2. The stress tensor sensor unit consists of a cube-shaped rigid body that has normal stress sensors V_i placed on each corner of the rigid cubic body in the center of a square elastic body. It is embedded in a linear elastic body.

Suppose a uniform deformation is given to the elastic body, and that the rigid body locally disturbs the stress field around it. Let the stress tensor components around the origine σ_{zz0} , σ_{zx0} , σ_{xx0} , and σ_{xz0} , and consider the gradient of the normal stress

$$\frac{\partial \sigma_{zz}}{\partial x}, \frac{\partial \sigma_{zz}}{\partial z}, \frac{\partial \sigma_{xz}}{\partial z} \text{ and } \frac{\partial \sigma_{xx}}{\partial x}. \quad (3)$$

When the even normal stress σ_{zz0} (Fig.3a) is applied to the surface of sensor unit (other stress components and

the gradients are equal to zero), from the geometric symmetry, the relationship of the normal stress sensor's output $V_1, V_2, V_3, V_4, V_5, V_6, V_7$, and V_8 to σ_{zz0} are expressed as following equations. The constants a and b in the equations depend on the Young's modulus, poisson's ratio and the shape of the rigid body.

$$V_1 = V_2 = V_3 = V_4 = a\sigma_{zz0} \quad (4)$$

$$V_5 = V_6 = V_7 = V_8 = -b\sigma_{zz0} \quad (5)$$

If we apply the similar analysis to the other components σ_{xx0} , σ_{zx0} (Fig.3b), σ_{xz0} and the gradient of normal stress σ_{zz} , from linear elasticity, the relationship between sensor outputs and the stress around the sensor chip (the rigid body) are expressed as following equations. The constants c, d, \dots, g and h are decided by the Young's modulus, poisson's ratio and the shape of sensor. The constant l is the length of each side of the cube.

$$\begin{pmatrix} V_1 \\ V_2 \\ V_3 \\ V_4 \\ V_5 \\ V_6 \\ V_7 \\ V_8 \end{pmatrix} = \begin{pmatrix} a & -c & -b & -d & -el & -gl & fl & hl \\ a & c & -b & d & el & -gl & fl & -hl \\ a & c & -b & d & -el & gl & -fl & hl \\ a & -c & -b & -d & el & gl & -fl & -hl \\ -b & -d & a & -c & fl & hl & -el & -gl \\ -b & d & a & c & fl & -hl & el & -gl \\ -b & d & a & c & -fl & hl & -el & gl \\ -b & -d & a & -c & -fl & -hl & el & gl \end{pmatrix} \begin{pmatrix} \sigma_{zz0} \\ \sigma_{zx0} \\ \sigma_{xz0} \\ \sigma_{xx0} \\ \frac{\partial \sigma_{zz}}{\partial x} \\ \frac{\partial \sigma_{zz}}{\partial z} \\ \frac{\partial \sigma_{xz}}{\partial z} \\ \frac{\partial \sigma_{xx}}{\partial x} \end{pmatrix} \quad (6)$$

Based on Eq. (6), we can reconstruct the stress applied to the elastic body as following equations using $\sigma_{zx} = \sigma_{xz}$.

$$\sigma_{zz0} = \frac{1}{4(a^2 - b^2)} \left(a \sum_{i=1}^4 V_i + b \sum_{i=5}^8 V_i \right) \quad (7)$$

$$\sigma_{xx0} = \frac{1}{4(a^2 - b^2)} \left(a \sum_{i=5}^8 V_i + b \sum_{i=1}^4 V_i \right) \quad (8)$$

$$\sigma_{zx0} = \sigma_{xz0} = -\frac{1}{4c} (V_1 - V_2 - V_3 + V_4) \quad (9)$$

$$\frac{\partial \sigma_{zz}}{\partial x} = -\frac{1}{4(eg - fh)l} \{g(V_1 - V_2 + V_3 - V_4) + h(V_5 + V_6 - V_7 - V_8)\} \quad (10)$$

$$\frac{\partial \sigma_{xz}}{\partial z} = -\frac{1}{4(eg - fh)l} \{h(V_1 + V_2 - V_3 - V_4) + g(V_5 - V_6 + V_7 - V_8)\} \quad (11)$$

$$\frac{\partial \sigma_{zz}}{\partial z} = -\frac{1}{4(eg - fh)l} \{e(V_1 + V_2 - V_3 - V_4) + f(V_5 - V_6 + V_7 - V_8)\} \quad (12)$$

$$\frac{\partial \sigma_{xx}}{\partial x} = -\frac{1}{4(eg - fh)l} \{f(V_1 - V_2 + V_3 - V_4) + e(V_5 + V_6 - V_7 - V_8)\} \quad (13)$$

The equations show that we can sense the stress tensor around the sensing chip and the gradient of the normal stress are obtained from the sensor outputs. In this sensing principle the second problem pointed out in Introduction has been solved.

An important feature of the sensing is that the ratios among a, b, c , and d are independent of the sensor size l .

Therefore the ratio of the SN ratios between the normal stress sensing and the shear stress sensing is independent of the scale l . On the other hand, the coefficients between the sensor outputs and the stress gradients include the scale parameter l . It means that the sensor outputs become insensitive to the stress gradients when the sensor size becomes small. Therefore the second problem in Introduction is a minor one for a micro STS.

3. PROTOTYPE

For fundamental experiments to confirm the principle of the stress tensor measurement, we fabricated the sensor which measured V_1 , V_2 , V_3 , and V_4 described in the foregoing chapter (Fig.4).

At first, the center cube of the sensor unit composed of an acrylic cube (8 mm × 9 mm) and four capacitive stress sensors placed on the corner of the cube. Each capacitive stress sensor consisted of a couple of phosphor bronze electrodes. The thickness of the electrodes was 0.2 mm. The outer electrode's size is 9 mm × 9 mm. The inner's are 4 mm × 9 mm. A polyimide film (1 mm width) was sandwiched between two pieces of electrodes as a prop and the distance between the electrodes was 25 μm. Proportional to strength of the normal stress applied to the outer electrodes, the distance and the capacitance between the electrodes changed. Because this design is for the artificial skin of the robot, we regarded the load of 300gf before and after as the upper limit of the measurement range. We could change the measurement range depending on the thickness of the GND electrode. We have the freedom about the Young's modulus of silicone rubber influencing the softness of the whole sensor element.

One of the electrodes was connected to GND and the other was connected to the input of a Schmitt inverter so that Schmitt inverter oscillator was formed. The oscillation frequency of the RC oscillator was determined by the capacitance of the normal stress sensors. The frequency f of the oscillator and the distance between the electrodes d have the following relationship

$$f = \frac{k}{RC} = \frac{k}{R(\varepsilon'S + C'd)}d, \quad (14)$$

where ε' is the dielectric constant of the air, S is the area of the electrode, R is the feedback resistance, C' is the parasitic capacitance and k is a constant. When normal stress is applied to the stress sensor, the oscillation frequency variation Δf , the distance variation Δd and the applied normal stress σ have the following relationship

$$\sigma = \frac{E}{d} \Delta d = -\frac{Ek}{dR} \frac{(C'd + \varepsilon'S)^2}{\varepsilon'S} \Delta f, \quad (15)$$

where E is the virtual Young's modulus of the phosphor bronze cantilever. When Δd is enough small, σ is proportional to Δf . Therefore sensor outputs V_i in Fig.2

corresponded to each frequency variation Δf_i .

At last, the center cube was embedded in a 30 mm × 30 mm square-shaped silicone rubber (KE-1308 Shin-Etsu Chemical Co. Ltd), and these are adhered (Fig.5).

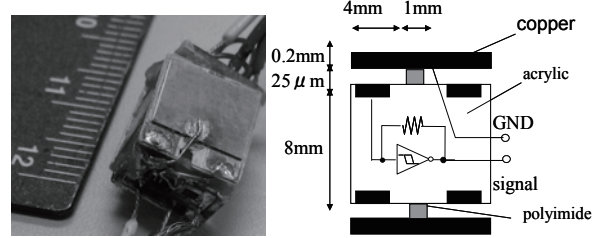


Fig.4 The photograph and schematic drawing of the center cube.

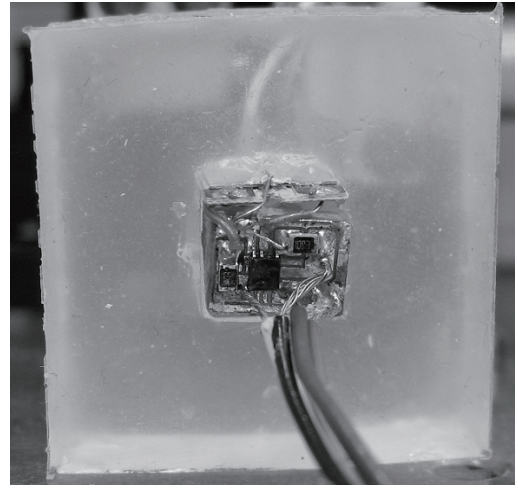


Fig.5 The structure of the prototype

4. EXPERIMENTS

4.1 Setup

Fig.6 shows experimental setup. Steel plates were placed at the top and bottom of the silicone. By moving the top and bottom steel plates in the z - and x -direction respectively, we applied the stress to the sensor. In this experiment, as the boundary condition of the side was free, " $\sigma_{xx} = 0$ ". Therefore because of Eq. (8),

$$\sum_{i=5}^8 V_i = -\frac{b}{a} \sum_{i=1}^4 V_i. \quad (16)$$

And substituting this equation to Eq. (7),

$$\sigma_{z0} = \frac{1}{4(a^2 - b^2)} \left(a - \frac{b^2}{a} \right) \sum_{i=1}^4 V_i = \frac{1}{4a} \sum_{i=1}^4 V_i. \quad (17)$$

In the same way about the shear stress and the gradient of the normal stress,

$$\sigma_{zx0} = \sigma_{xz0} = -\frac{1}{4c} (V_1 - V_2 - V_3 + V_4), \quad (18)$$

$$\frac{\partial \sigma_{zz}}{\partial x} = -\frac{1}{4el}(V_1 - V_2 + V_3 - V_4). \quad (19)$$

Therefore, we can reasonably define the stress tensor sensor outputs P_{normal} as the average of normal stress as follows.

$$P_{\text{normal}} = -\Delta f_1 - \Delta f_2 - \Delta f_3 - \Delta f_4 \quad (20)$$

Likewise the shear stress P_{shear} and the gradient of the normal stress P_{grad} are given as,

$$P_{\text{shear}} = -\Delta f_1 + \Delta f_2 + \Delta f_3 - \Delta f_4. \quad (21)$$

$$P_{\text{grad}} = \Delta f_1 - \Delta f_2 + \Delta f_3 - \Delta f_4. \quad (22)$$

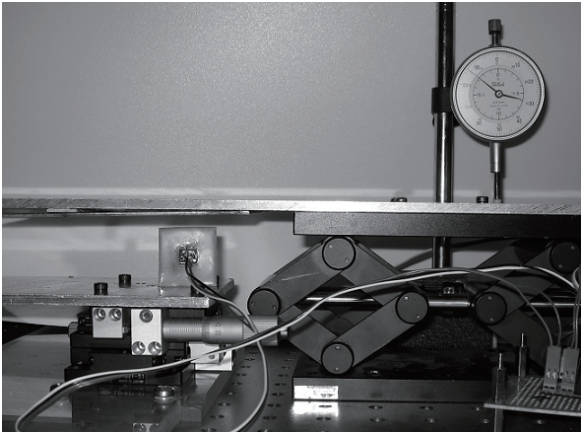


Fig.6 The experimental setup.

4.2 Experiments

Even normal stress

First, only the top plate was moved in the z -direction. Fig.7 shows the results. The horizontal axis represents the displacement of the top steel plate. The vertical axis represents P_{normal} , P_{shear} and P_{grad} .

While P_{normal} increases proportional to the plate displacement in the z -direction increasing, P_{shear} and P_{grad} are nearly zero. When P_{normal} was approximated by linear, the square of the correlation factor was 0.9997.

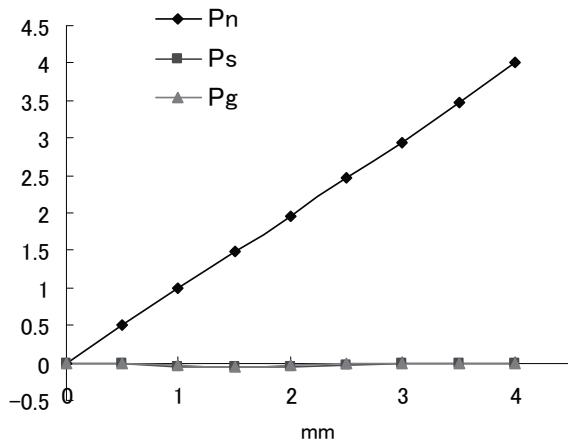


Fig.7 The sensor outputs for the even normal stress.

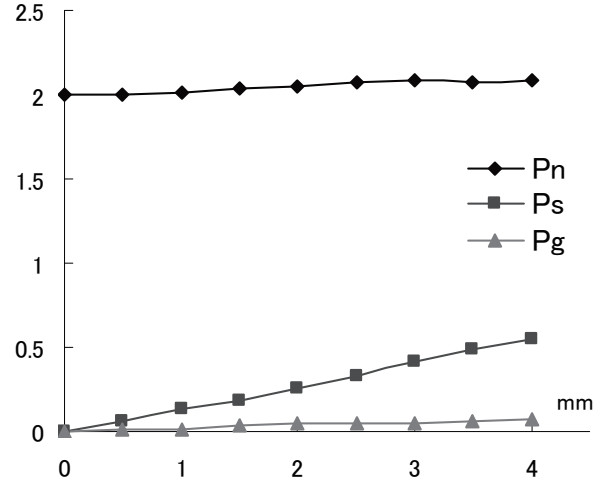


Fig.8 The sensor outputs for the shear stress.

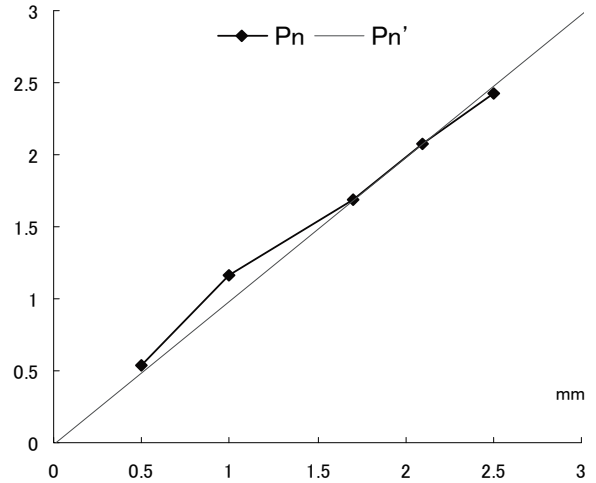


Fig.9 The average of normal stress.

Shear stress

After the silicone was initially strained by moving the top plate in the z -direction up to 2 mm, only the bottom plate was moved in the x -direction. In this case, it is assumed that shear stress was uniformly applied on the top and bottom surface of the silicone rubber.

Fig. 8 shows the results. The horizontal axis represents the displacement of the bottom steel plate. P_{shear} increases proportional to the plate displacement increasing in the x -direction, while P_{normal} and P_{grad} does not seem to change. When P_{normal} and P_{shear} were approximated respectively by linear, the square of the correlation factor was 0.9469 and 0.998.

Tilt normal stress

At last, in order to apply normal stress varied linearly, we made slope on the top plate. The bottom plate was fixed and only the top plate was moved in the z -direction till the whole silicone top surface adhered with the slope. In Fig.9, the horizontal axis represents the average of z -displacement of the silicone top surface, and the vertical axis represents the output P_{normal} (P_n).

The line P_n' shows the theoretical values. In Fig.10, the horizontal axis represents the degree of slop angle, and we plotted the outputs of P_{shear} and P_{grad} . As the theory predicted, P_{grad} changed according to the angle change, while P_{shear} was relatively constant.

Transmission Layer, Proc. 4th International Conference on Networked Sensing Systems (INSS 2007), June 6-8, Braunschweig, Germany, pp. 201-206, 2007.

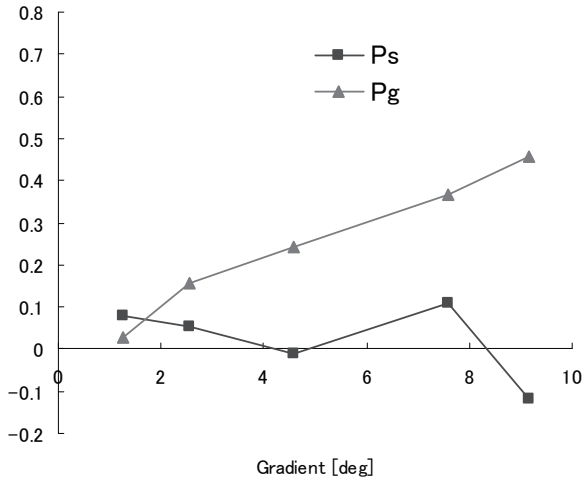


Fig.10 The sensor outputs for the varying gradient.

5. SUMMARY

We proposed a stress tensor sensor that is embedded in an elastic body and measure the stress tensor around it. The theory to decompose the shear stress and the normal stress gradient was given. The theory was examined by a prototype sensor. The experimental results showed that the sensor can measure normal and shear stress at one time. Also, the sensor can distinguish shear stress and linearly varied normal stress.

In our future design, the electrical power and the data signals will be transmitted without wires.

REFERENCES

- [1] M. H. Lee and H. R. Nicholls, "Tactile sensing for mechatronics --a state of the art survey", *Mechatronics* 9, pp.1-31, 1999.
- [2] http://www.nitta.co.jp/product/mechasen/sensor/tactile_system_sensor.html
- [3] M. Shimojo, A. Namiki, M. Ishikawa, R. Makino, and K. Mabuchi A Tactile Sensor Sheet Using Pressure Conductive Rubber With Electrical-Wires Stitched Method, *IEEE SENSORS JOURNAL*, VOL. 4, NO. 5, OCTOBER 2004]
- [4] M. Hakozaiki and H. Shinoda, "Digital Tactile Sensing Elements Chommunicating through Conductive Skin Layers," *Proc of te 2002 IEEE Transactions on Robotics and Automation*, 2002,
- [5] H. Shinoda, K. Matsumoto and S. Ando, "Tactile Sensing Based on Acoustic Resonance Tensor Cell," *Proc of TRANSDUCERS '97*, Vol.1, pp. 129-132, 1997.
- [6] H. Shinoda, Y. Makino, N. Yamahira, and H. Itai: Surface Sensor Network Using Inductive Signal